Supplemental information

Inducible super-enhancers are organized by canonical signal-specific transcription factor binding elements

Dóra Bojcsuk, Gergely Nagy and Balint L. Balint

SUPPLEMENTARY FIGURES (page 2-11)

SUPPLEMENTARY TABLES (page 12-14)

SUPPLEMENTAL REFERENCES (page 15-16)

Figure S1.

A

Minimum overlap	Overlapping ERα peaks
8	**4 387**
7	7 606
6	11 396
5	16 864
4	24 906
3	36 234
2	56 931

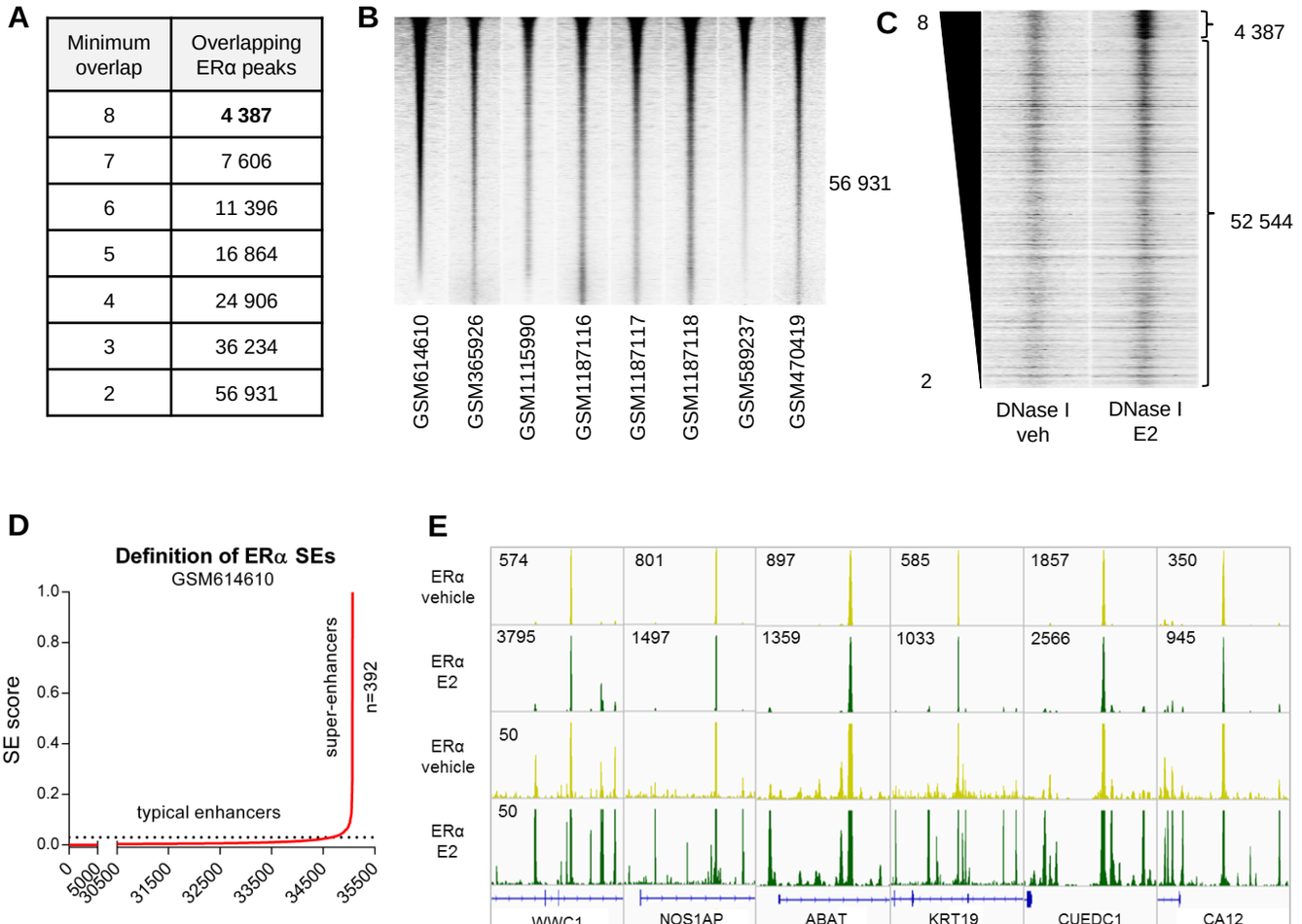

Figure S1. Comparison of ERα ChIP-seq binding sites upon E2 treatment.

(A) Number of the common ERα peaks between eight different ChIP-seq samples after various overlapping criteria.
(B) Read distribution plot represents the 56,931 ERα peaks which could be predicted from at least two samples. Peaks were sorted by the calculated RPKM values of GSM614610 experiment.
(C) Read distribution plot demonstrates the signal intensity of DNase I hypersensitivity at the sites of the 56,931 ERα peaks sorted by the amount of overlap between the eight experiments (from 8 to 2 samples). Reads were calculated from GSM614610 experiment.
(D) Definiton of ERα SEs. Enhancers with a slope greater than 1 are considered as SEs.
(E) IGV snapshot of ERα ChIP-seq coverage representing six ERα SEs upon vehicle (veh) and estradiol (E2) treatments. The interval scales are autoscale in the first two tracks and 50 in the last two tracks.
(F-G) ERα densities upon vehicle or E2 treatment in the deciles defined by ERα recruitment at those SE regions showing read enrichment.

Figure S2.

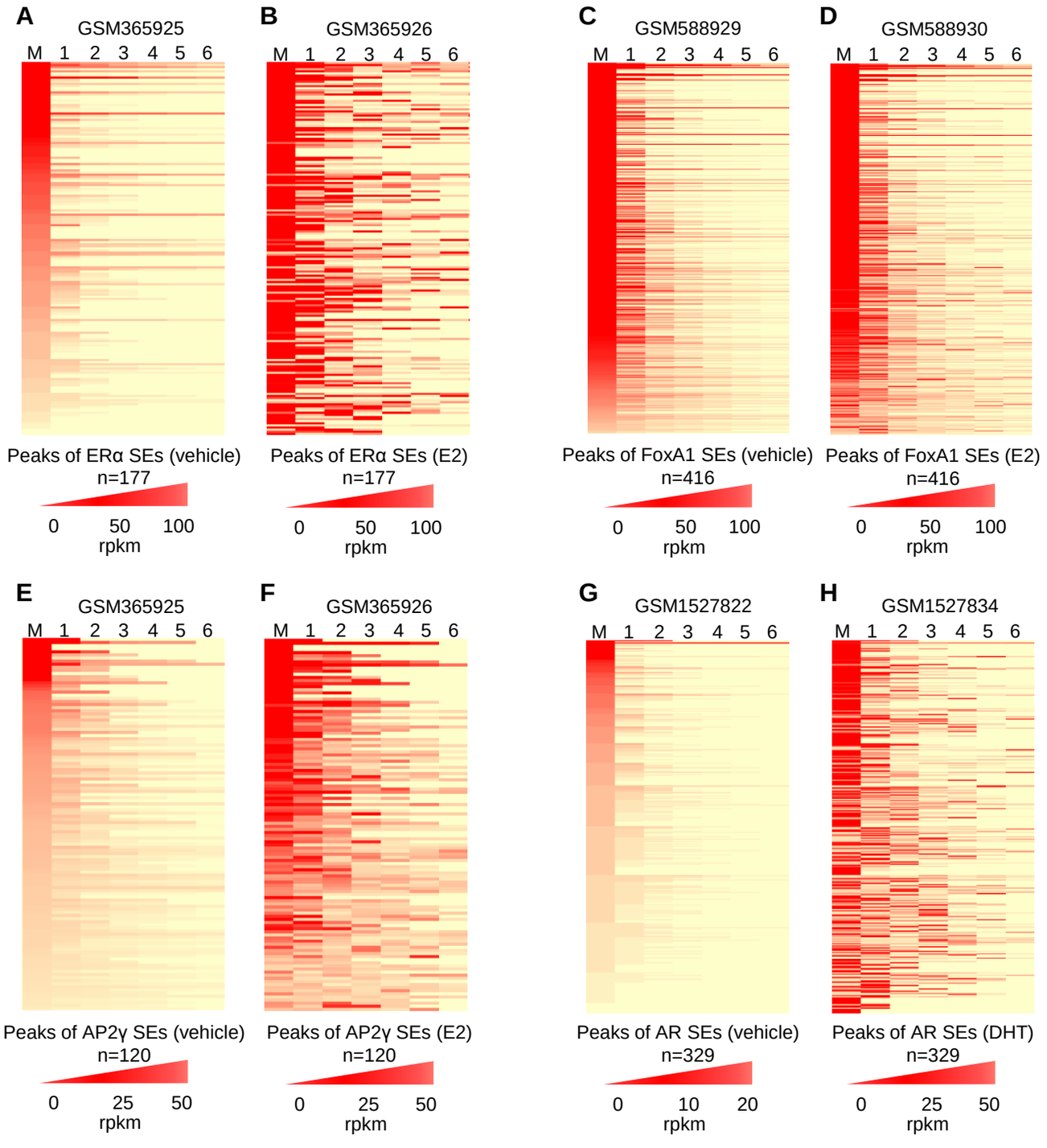

Figure S2. Appearing daughter enhancers are recruited neirby to mother enhancers upon treatment.

(A-B) ERα tag densities of mother (M) and the top 6 daughter enhancers (1-6) forming super-enhancers in vehicle (veh) and estradiol (E2) treated MCF-7 cells.
(C-D) FoxA1 tag densities of mother (M) and the top 6 daughter enhancers (1-6) forming super-enhancers in vehicle (veh) and E2 treated MCF-7 cells.
(E-F) AP2γ tag densities of mother (M) and the top 6 daughter enhancers (1-6) forming super-enhancers in vehicle (veh) and E2 treated MCF-7 cells.
(G-H) AR tag densities of mother (M) and the top 6 daughter enhancers (1-6) forming super-enhancers in vehicle (veh) and dihydrotestosterone (DHT) treated LNCaP cells.

Enhancers were vertically sorted based on the RPKM values of the mother enhancers (in the first row), and the individual enhancers within a SE region were subsequently horizontally aligned based on read enrichment in the vehicle-treated samples.

Figure S2.

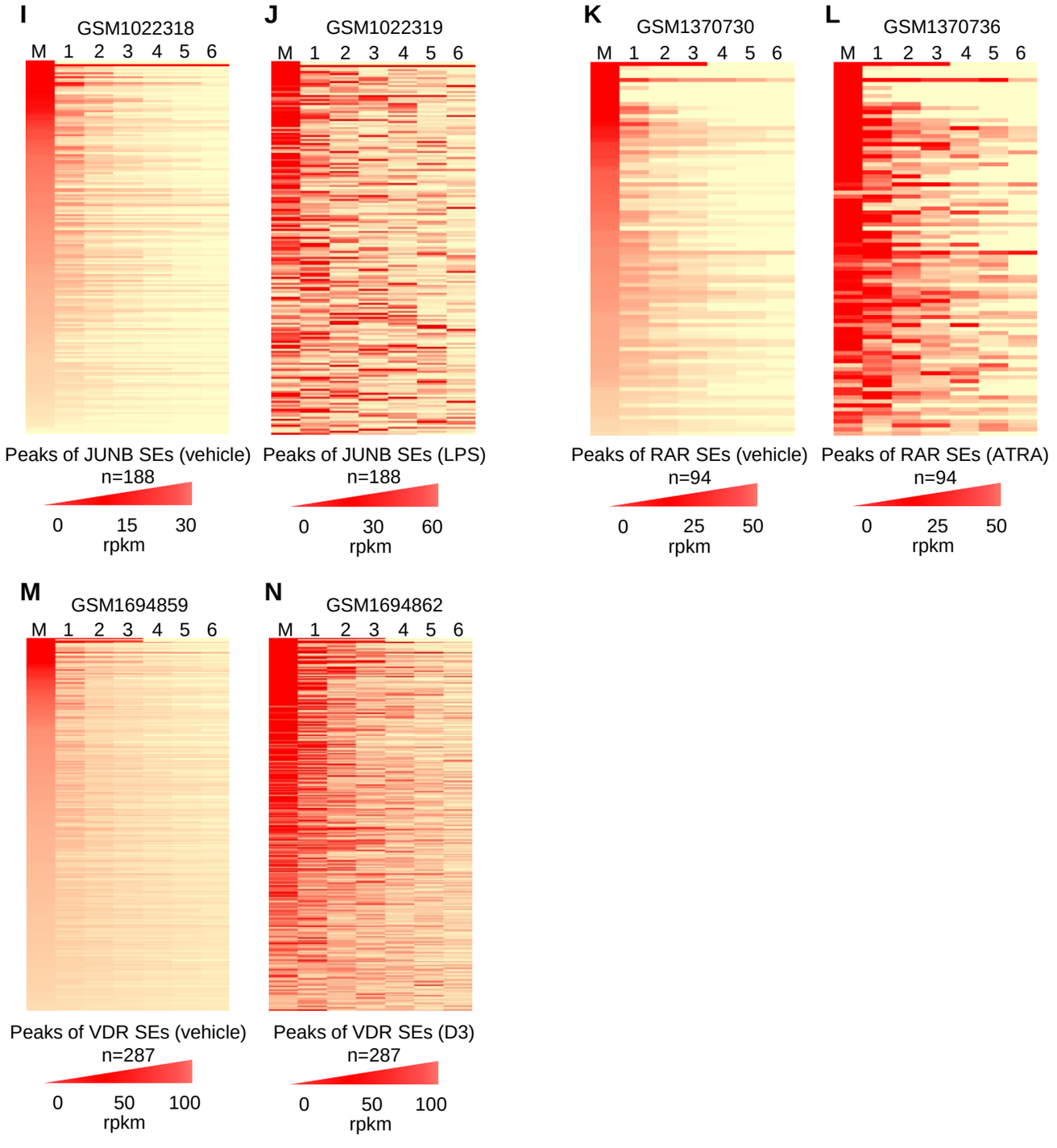

Figure S2. Appearing daughter enhancers are recruited neirby to mother enhancers upon treatment.

(I-J) JUNB (AP-1) tag densities of mother (M) and the top 6 daughter enhancers (1-6) forming super-enhancers in vehicle (veh) and lipopolysaccharide (LPS) treated bone marrow-derived machrophages (BMDMs).
(K-L) RAR tag densities of mother (M) and the top 6 daughter enhancers (1-6) forming super-enhancers in vehicle (veh) and all-trans retionoic acid (ATRA) treated F9 cells.
(M-N) VDR tag densities of mother (M) and the top 6 daughter enhancers (1-6) forming super-enhancers in vehicle (veh) and cholecalciferol (D3) treated mouse intestinal epithelial cells.

Enhancers were vertically sorted based on the RPKM values of the mother enhancers (in the first row), and the individual enhancers within a SE region were subsequently horizontally aligned based on read enrichment in the vehicle-treated samples.

Figure S3.

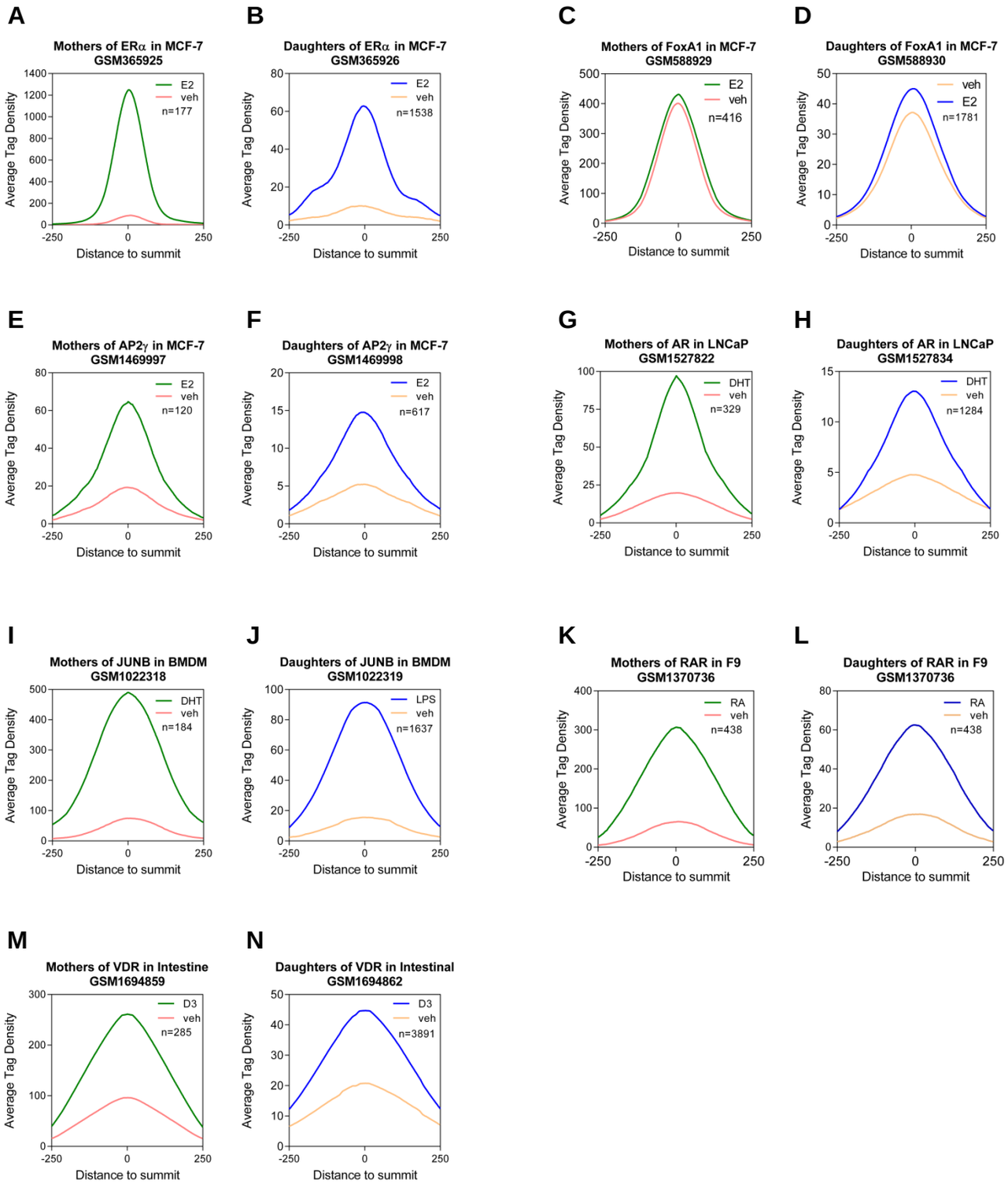

Figure S3. Mother enhancers show larger tag density before treatment than the daughter enhancers upon treatment.

Histograms show the average tag density of ERα **(A-B)**, FoxA1 **(C-D)** and AP2γ **(E-F)** mother and daughter enhancers in vehicle (veh) and estradiol (E2) treated MCF-7 cells;
(G-H) AR mother and daughter peaks in vehicle (veh) and dihydrotestosterone (DHT) treated LNCaP cells;
(I-J) JUNB mother and daughter peaks in vehicle (veh) and lipopolysaccharide (LPS) treated bone marrow-derived machrophages (BMDMs);
(K-L) RAR mother and daughter peaks in vehicle (veh) and all-trans retionoic acid (ATRA) treated F9 cells;
(M-N) VDR mother and daughter peaks in vehicle (veh) and cholecalciferol (D3) treated mouse intestinal epithelial cells.

Figure S4.

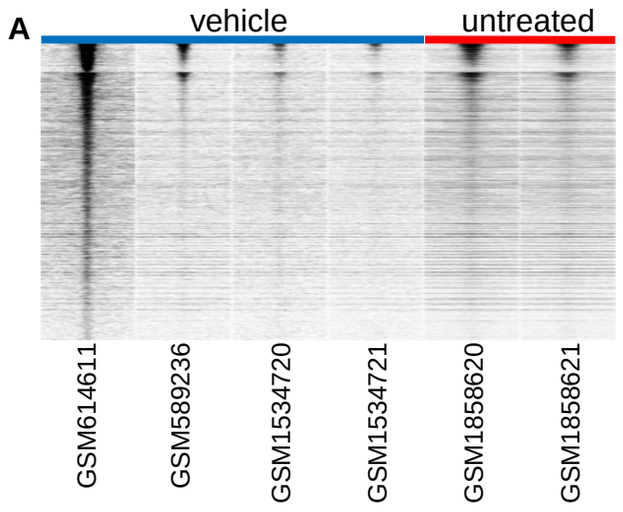

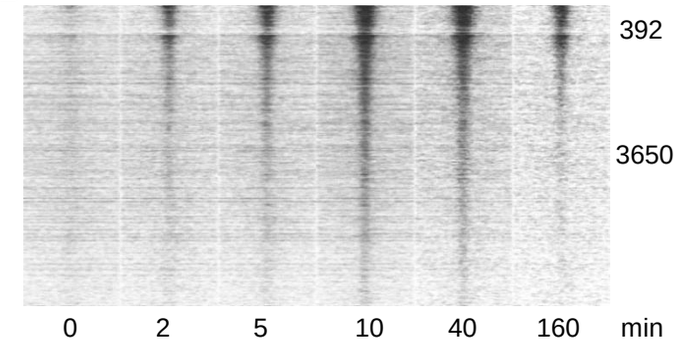

C

Experiment	IP efficiency
GSM1325246 – 0 min	1,17
GSM1325247 – 2 min	2,00
GSM1325248 – 5 min	2,50
GSM1325249 – 10 min	6,39
GSM1325250 – 40 min	7,51
GSM1325251 – 160 min	2,67

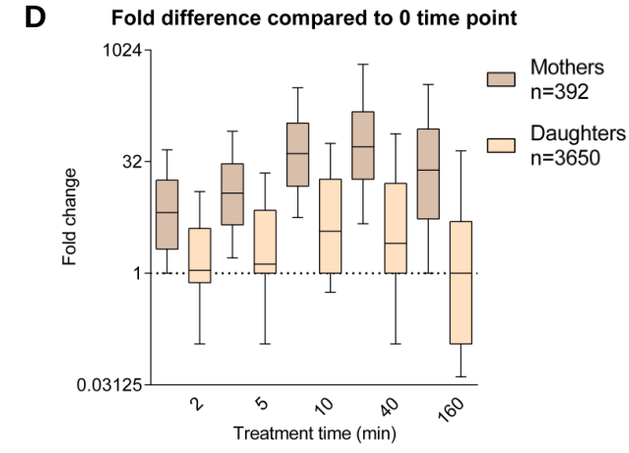

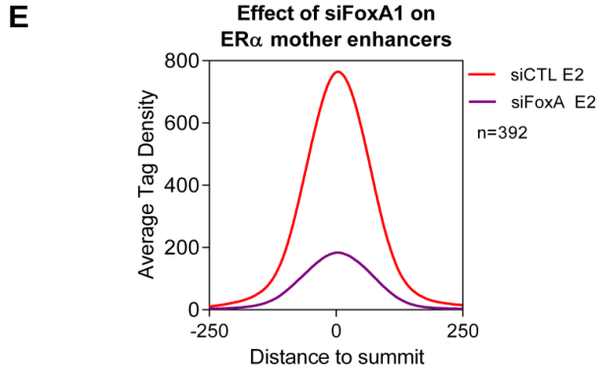

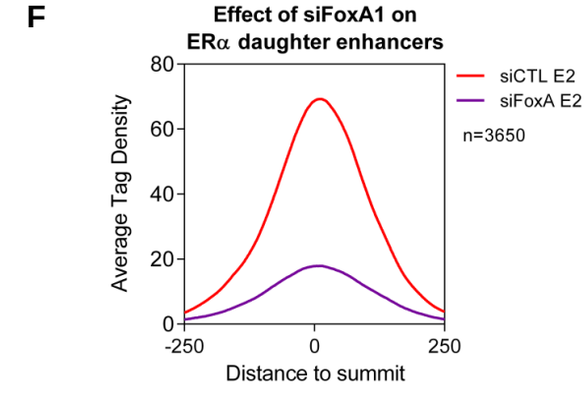

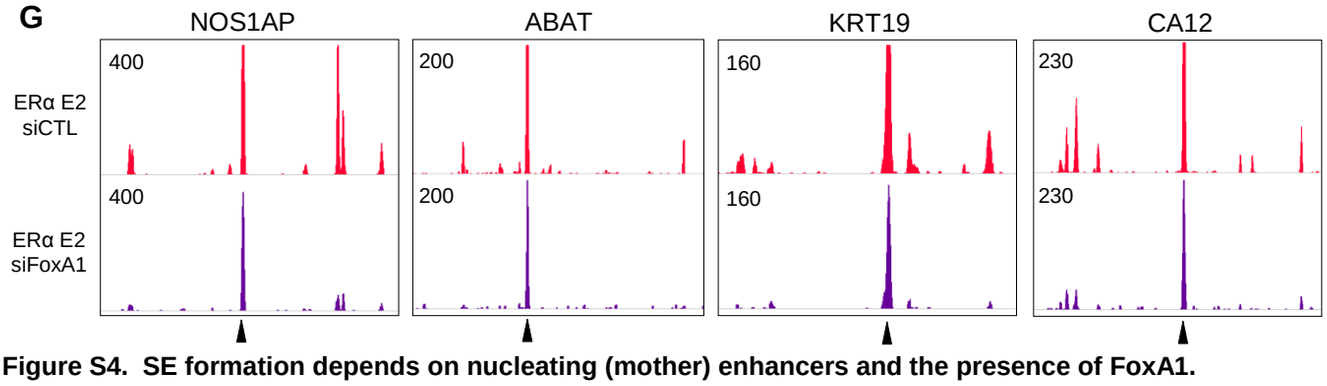

Figure S4. SE formation depends on nucleating (mother) enhancers and the presence of FoxA1.

(A) Read distribution plots of ERα mother (392) and daughter (3650) enhancers upon vehicle treatment or without any treatment (untreated), and **(B)** upon E2-treatment in different time points (0, 2, 5, 10, 40, 160 min) relative to ERα-bound SE peaks in 2 kb frames. **(C)** Calculated IP-efficiency of the used samples. **(D)** Box plot represent fold differences of ERα enhancers compared to the 0 time point. Histograms show the average tag density of ERα **(E)** mother and **(F)** daughter enhancers derived from E2-treated siCTL and siFoxA1 ChIP-seq experiments. **(G)** IGV snapshot of ERα ChIP-seq coverage, representing four E2-treated ERα SEs before (siCTL) and after the silencing of FoxA1 (siFoxA1).

Figure S5.

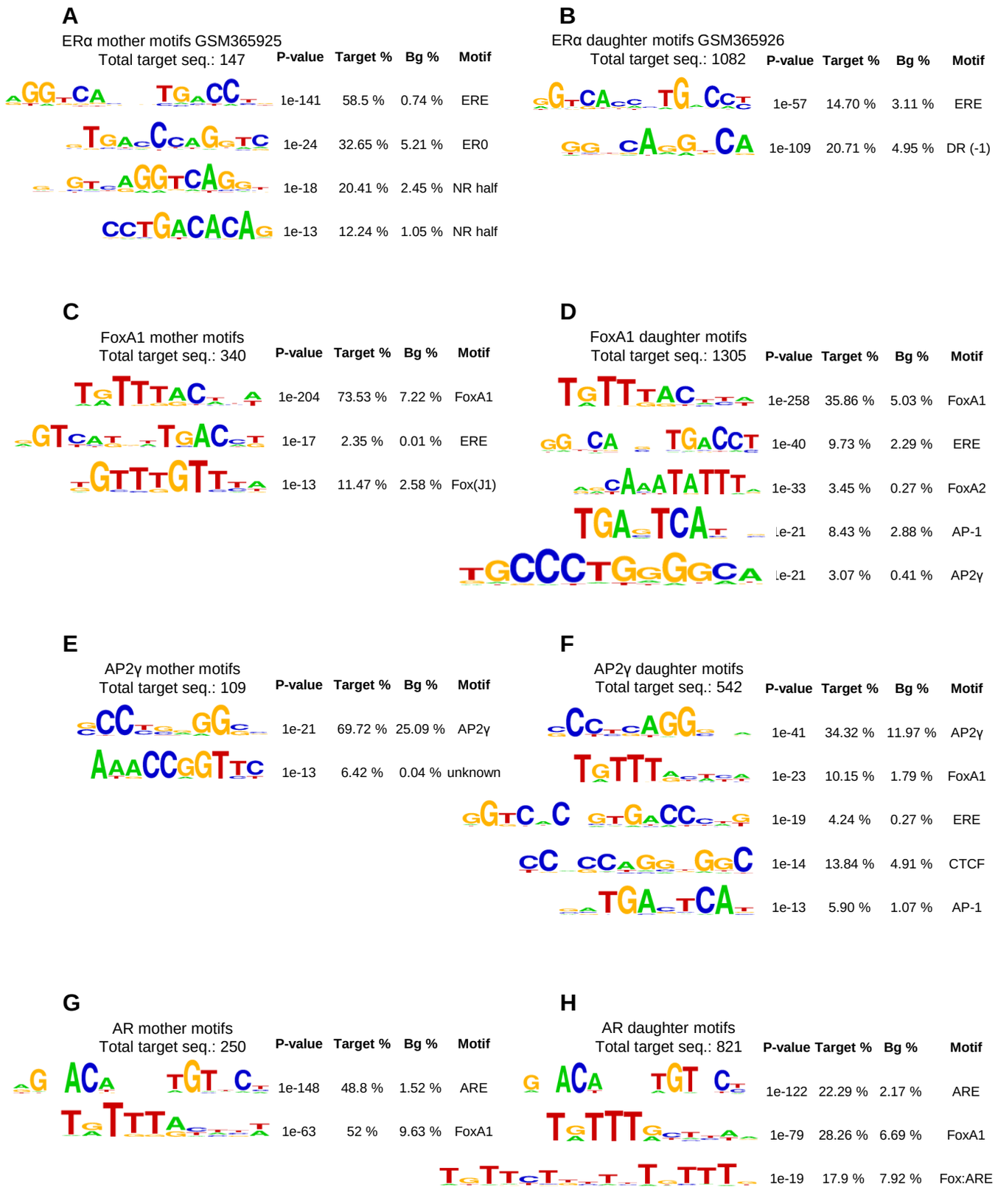

Figure S5. Canonical elements provide higher DNA-binding affinity than non-canonical elements.

Motif enrichment analysis under the mother and daughter enhancers of ERα **(A-B)**, FoxA1 **(C-D)**, AP2γ **(E-F)** and AR **(G-H)**. The P-value and target and background (Bg) percentages are included for each motif.

Figure S5.

I

JUNB mother motifs
Total target seq.: 187

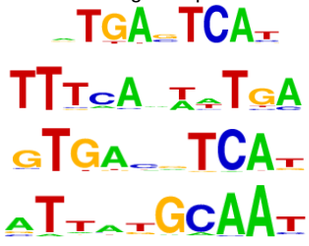

P-value	Target %	Bg %	Motif
1e-77	48.13 %	3.52 %	AP-1
1e-21	12.83 %	0.78 %	AICE
1e-15	20.32 %	3.96 %	CRE
1e-14	16.58 %	2.9 %	C/EBP

J

JUNB daughter motifs
Total target seq.: 1637

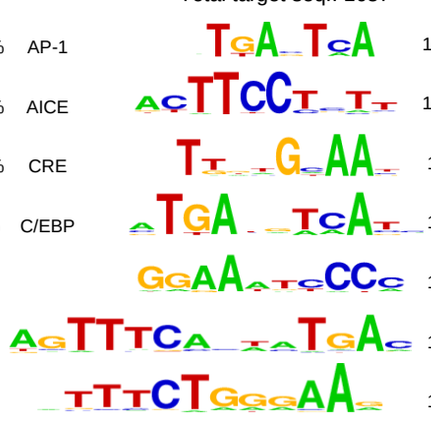

P-value	Target %	Bg %	Motif
1e-256	29.14 %	4.07 %	AP-1
1e-109	20.71 %	4.95 %	PU.1
1e-59	19.30 %	6.95 %	C/EBP
1e-39	11.42 %	3.74 %	CRE
1e-38	10.14 %	3.10 %	NFkB
1e-23	4.09 %	0.78 %	AICE
1e-23	6.78 %	2.24 %	STAT

K

RAR mother motifs
Total target seq.: 93

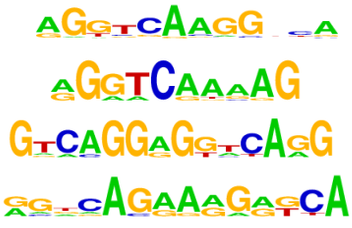

P-value	Target %	Bg %	Motif
1e-50	49.46 %	2.12 %	DR0
1e-24	31.18 %	2.28 %	DR2
1e-23	12.9 %	0.07%	DR2
1e-15	20.32 %	3.96 %	DR3

L

RAR daughter motifs
Total target seq.: 438

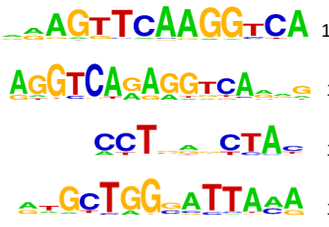

P-value	Target %	Bg %	Motif
1e-145	31.28 %	1.26 %	DR0
1e-23	8.45 %	0.88 %	DR1
1e-13	18.04 %	7.00 %	unknown
1e-13	10.5 %	2.78 %	unknown

M

VDR mother motifs
Total target seq.: 285

P-value	Target %	Bg %	Motif
1e-101	45.96 %	4.05 %	VDRE
1e-21	14.74 %	2.16 %	NR half
1e-14	5.96 %	0.38%	GATA
1e-14	16.84 %	4.47 %	NR half

N

VDR daughter motifs
Total target seq.: 3891

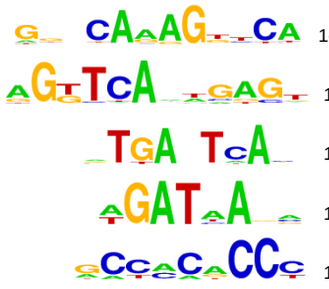

P-value	Target %	Bg %	Motif
1e-152	22.23 %	8.40 %	DR1
1e-52	8.4 %	3.21 %	VDRE
1e-47	5.27 %	1.58 %	AP-1
1e-46	9.69 %	4.28 %	GATA
1e-35	16.94 %	10.30%	KLF

Figure S5. Canonical elements provide higher DNA-binding affinity than non-canonical elements.

Motif enrichment analysis under the mother and daughter enhancers of JUNB **(I-J)**, RAR **(K-L)** and VDR **(M-N)**. The P-value and target and background (Bg) percentages are included for each motif.

Figure S6.

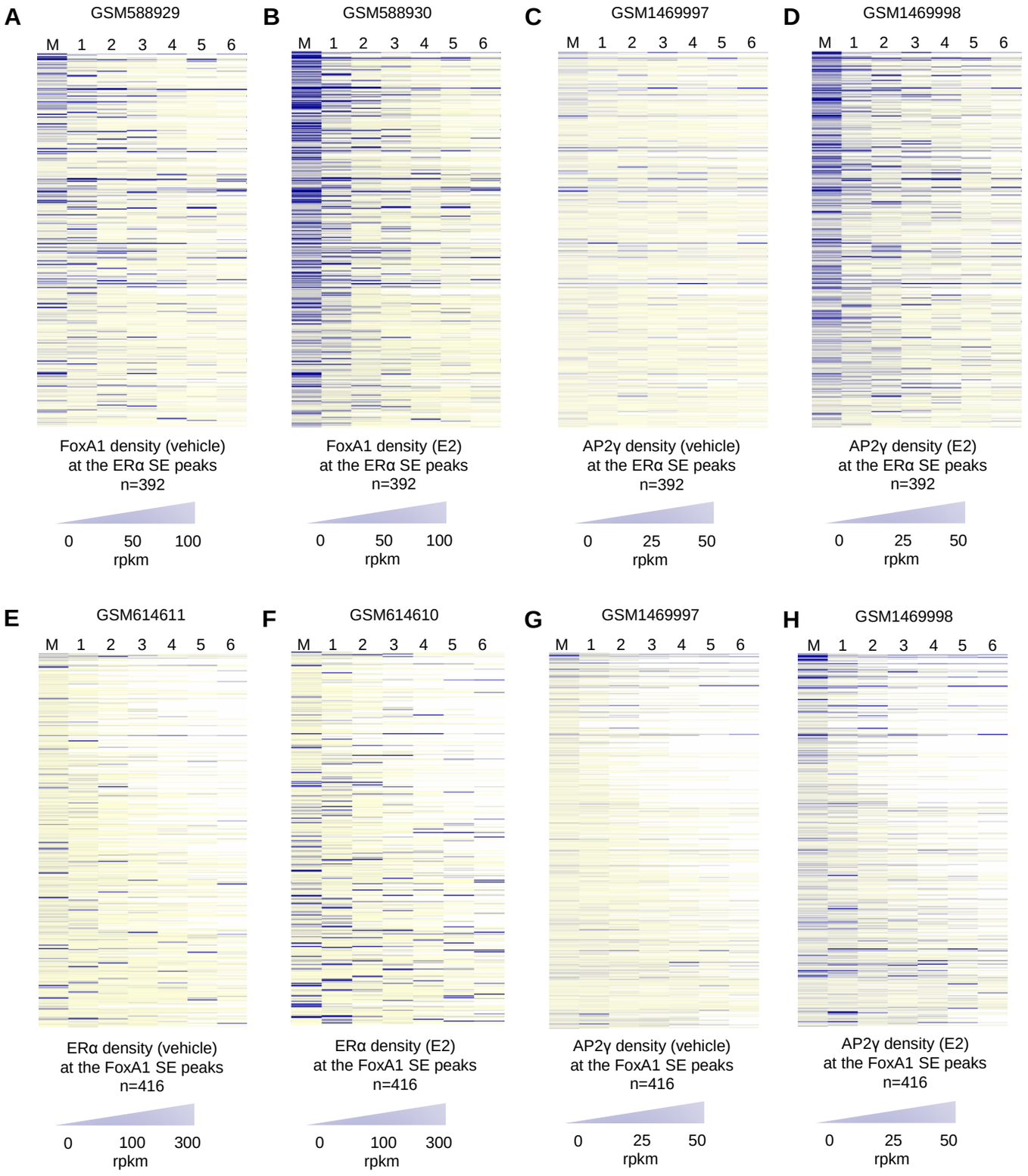

Figure S6. Recruitment of ERα, FoxA1 and AP2γ at each other's SEs.

Heatmaps represent the FoxA1 **(A-B)** and AP2γ **(C-D)** density at the ERα mother (M) and the top 6 daughter enhancers (1-6) forming super-enhancers in vehicle (veh) and estradiol (E2) treated MCF-7 cells.
ERα **(E-F)** and AP2γ **(G-H)** density at the FoxA1 mother (M) and the top 6 daughter enhancers (1-6) forming super-enhancers in vehicle (veh) and estradiol (E2) treated MCF-7 cells.

Enhancers were vertically sorted based on the RPKM values of the mother enhancers (in the first row), and the individual enhancers within a SE region were subsequently horizontally aligned based on read enrichment in the vehicle-treated samples.

Figure S6.

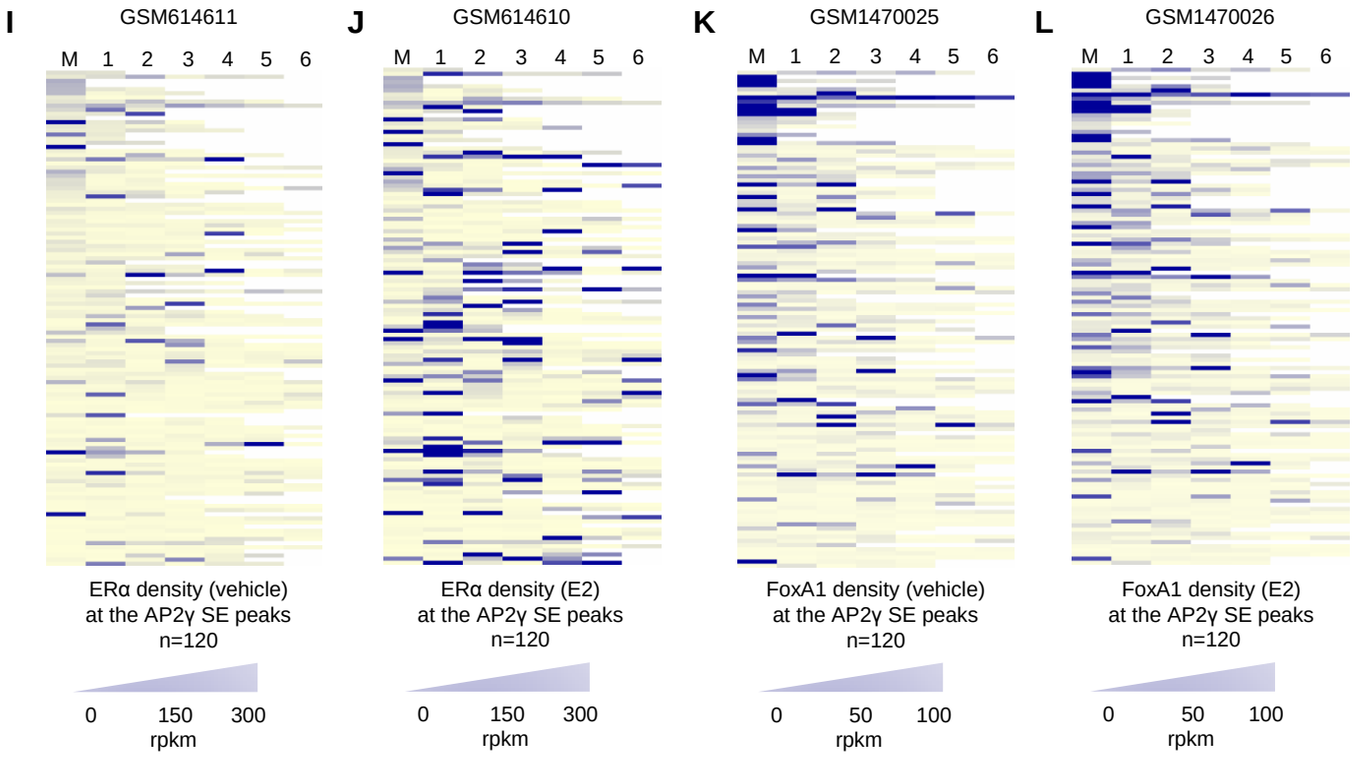

Figure S6. Recruitment of ERα, FoxA1 and AP2γ at each other's SEs.

Heatmaps represent the ERα **(I-J)** and FoxA1 **(K-L)** density at the AP2γ mother (M) and the top 6 daughter enhancers (1-6) forming super-enhancers in vehicle (veh) and estradiol (E2) treated MCF-7 cells.

Enhancers were vertically sorted based on the RPKM values of the mother enhancers (in the first row), and the individual enhancers within a SE region were subsequently horizontally aligned based on read enrichment in the vehicle-treated samples.

Figure S7.

A

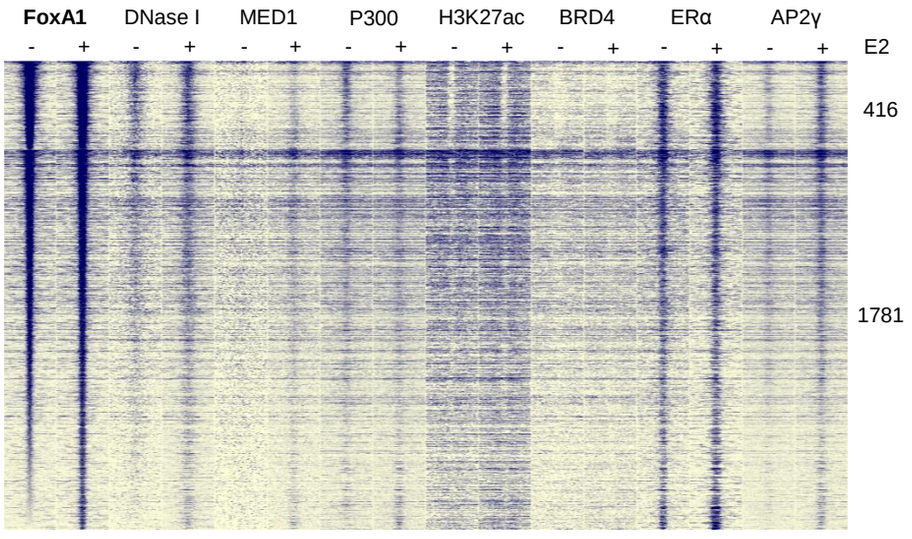

B

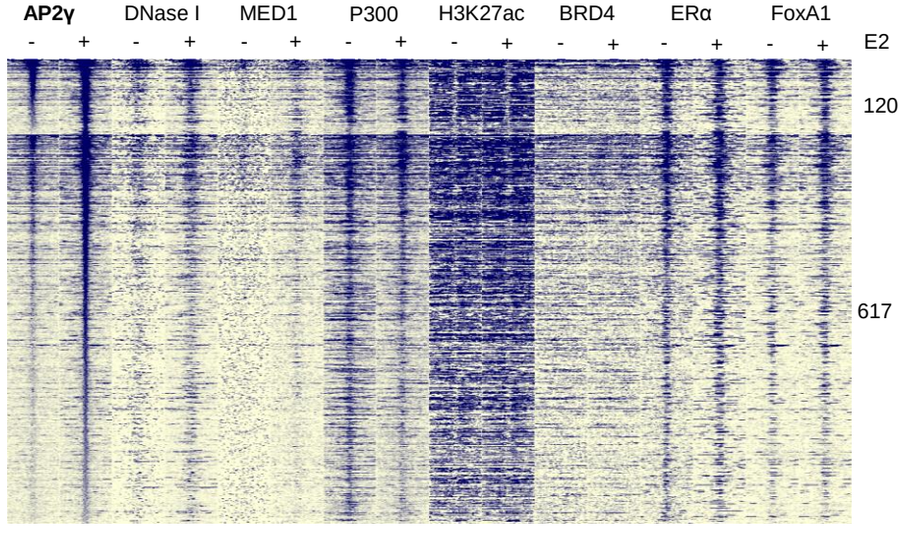

Figure S7. FoxA1 and AP2γ super-enhancers show active but not inducible presence of active marks and co-factors upon E2 treatment.

Read distribution plot of DNase I, MED1, P300, H3K27ac, BRD4, ERα and AP2γ or FoxA1 upon vehicle or E2 treatment, relative to FoxA1 **(A)** or AP2γ **(B)** SE peaks in 2 kb frames. The number of mother and daughter peaks, which are sorted according to FoxA1 **(A)** or AP2γ **(B)** tag density.

Table S1.

Transcription factor	Cell line	Treatment	Organism	GEO ID (vehicle)	GEO ID (treated)	Reference
ERα	MCF-7	E2	human	GSM614611	GSM614610	(1)
ERα	MCF-7	E2	human	GSM365925	GSM365926	(2)
FoxA1	MCF-7	E2	human	GSM588929	GSM588930	(3)
AP2γ	MCF-7	E2	human	GSM1469997	GSM1469998	(4)
AR	LNCaP	DHT	human	GSM1527822	GSM1527834	(5)
JUNB	BMDM	LPS	mouse	GSM1022318	GSM1022319	(6)
RAR	F9	RA	mouse	GSM1370730	GSM1370736	(7)
VDR	Intestinal	D3	mouse	GSM1694859	GSM1694862	(8)

Table S1. Table of used transcription factor ChIP-seq samples.

Table contains informations about transcription factor ChIP-seq samples that have been used to the basic analyses to determine mother-daughter phenomenon. Columns represent the examined transcription factors, the cell line in which the interested TF/binding events was/were investigated, type of the treatment and organism, Gene Expression Omnibus (GEO) IDs of the samples before (vehicle) and after the treatment (treated).

Table S2.

GEO ID	E2 treatment	MACS2 peaks w/o artifacts	Predicted SEs	Peaks within SEs	Overlapping SEs with consensus	Reference
GSM614610	100 nM, 45 min	74 697	392	4 042	379 (96.6 %)	(1)
GSM365926	10 nM, 1 hr	82 777	270	1124	269 (99.6 %)	(2)
GSM1187116	10 nM, 45 min	46 423	342	1251	311 (90.9%)	(9)
GSM1187117	10 nM, 45 min	41 164	483	1834	455 (94.2 %)	
GSM1187118	10 nM, 45 min	33 306	418	1394	393 (94 %)	
GSM1115990	100 nM, 1 hr	31 964	186	761	179 (96.2%)	(10)
GSM589237	100 nM, 45 min	13 052	152	480	151 (99.3 %)	(11)
GSM470419	10 nM, 45 min	28 936	208	586	203 (97.6%)	(12)

Table S2. Estradiol-treated (E2) ERα ChIP-seq samples used for the comparative analysis.

Table contains the Gene expression Omnibus (GEO) IDs of eight publicly available ERα ChIP-seq samples derived from MCF-7 cell line; further the circumstances of E2-treatment; number of the predicted MACS2 peaks, from which the blacklisted genomic regions collected by ENCODE were removed; number of the predictable super-enhancers (SEs); number of the peaks within SEs and a percent value about how many SEs overlap with at least one peak(s) of the 4,387 consensus ERα binding sites.

Table S3.

(Transcription) factor	Cell line	Organism	GEO ID (vehicle)	GEO ID (E2 treated)	GEO ID (untreated)	GEO ID (tam/fulv)	Reference
MED1	MCF-7	human	GSM1469999	GSM1470000	-	-	(4)
P300	MCF-7	human	GSM1470013	GSM1470014	-	-	(4)
DNase I	MCF-7	human	GSM822389	GSM822390	-	-	(13)
H3K27ac	MCF-7	human	GSM1382472	GSM1382482	-	-	(14)
BRD4	MCF-7	human	GSM1348516	GSM1348519	-	-	(4)
ERα	MCF-7	human	GSM589236	-	-	-	(11)
ERα	MCF-7	human	GSM1534720	-	-	-	(15)
ERα	MCF-7	human	GSM1534721	-	-	-	
ERα	MCF-7	human	-	-	GSM1858620	-	(16)
ERα	MCF-7	human	-	-	GSM1858621	-	
ERα (0 min)	MCF-7	human	-	-	GSM1325246	-	(17)
ERα (2 min)	MCF-7	human	-	GSM1325247	-	-	
ERα (5 min)	MCF-7	human	-	GSM1325248	-	-	
ERα (10 min)	MCF-7	human	-	GSM1325249	-	-	
ERα (40 min)	MCF-7	human	-	GSM1325250	-	-	
ERα (160 min)	MCF-7	human	-	GSM1325251	-	-	
ERα (siFoxA1)	MCF-7	human	GSM631465	-	-	-	(18)
ERα (siFoxA1)	MCF-7	human	-	GSM631467	-	--	
ERα (tam/fulv)	MCF-7	human	GSM365925	-	-	-	(2)
ERα (tam/fulv)	MCF-7	human	-	GSM365926	-	-	
ERα (tamoxifen)	MCF-7	human	-	-	-	GSM365927	
ERα (fulvestrant)	MCF-7	human	-	-	-	GSM365928	

Table S3. Table of used ChIP-seq samples to characterize super-enhancers.

Table contains informations about ChIP-seq samples that have been used to the characterization of enhancers. Columns represent the examined factors, the cell line and organism in which the interested events were investigated, Gene Expression Omnibus (GEO) IDs, treatment type of ChIP-seq samples (vehicle, E2, untreated, tamoxifen or fulvestrant) and the related references.

Supplemental references

1. Schmidt,D., Schwalie,P.C., Ross-Innes,C.S., Hurtado,A., Brown,G.D., Carroll,J.S., Flicek,P. and Odom,D.T. (2010) A CTCF-independent role for cohesin in tissue-specific transcription. *Genome Res.*, **20**, 578–88.

2. Welboren,W.-J., van Driel,M.A., Janssen-Megens,E.M., van Heeringen,S.J., Sweep,F.C., Span,P.N. and Stunnenberg,H.G. (2009) ChIP-Seq of ERalpha and RNA polymerase II defines genes differentially responding to ligands. *EMBO J.*, **28**, 1418–28.

3. Tan,S.K., Lin,Z.H., Chang,C.W., Varang,V., Chng,K.R., Pan,Y.F., Yong,E.L., Sung,W.K., Sung,W.K. and Cheung,E. (2011) AP-2γ regulates oestrogen receptor-mediated long-range chromatin interaction and gene transcription. *EMBO J.*, **30**, 2569–81.

4. Liu,Z., Merkurjev,D., Yang,F., Li,W., Oh,S., Friedman,M.J., Song,X., Zhang,F., Ma,Q., Ohgi,K.A., *et al.* (2014) Enhancer Activation Requires trans-Recruitment of a Mega Transcription Factor Complex. *Cell*, **159**, 358–373.

5. Takayama,K., Suzuki,T., Tsutsumi,S., Fujimura,T., Urano,T., Takahashi,S., Homma,Y., Aburatani,H. and Inoue,S. (2015) RUNX1, an androgen- and EZH2-regulated gene, has differential roles in AR-dependent and -independent prostate cancer. *Oncotarget*, **6**, 2263–76.

6. Ostuni,R., Piccolo,V., Barozzi,I., Polletti,S., Termanini,A., Bonifacio,S., Curina,A., Prosperini,E., Ghisletti,S. and Natoli,G. (2013) Latent Enhancers Activated by Stimulation in Differentiated Cells. *Cell*, **152**, 157–171.

7. Chatagnon,A., Veber,P., Morin,V., Bedo,J., Triqueneaux,G., Sémon,M., Laudet,V., d'Alché-Buc,F. and Benoit,G. (2015) RAR/RXR binding dynamics distinguish pluripotency from differentiation associated cis-regulatory elements. *Nucleic Acids Res.*, **43**, 4833–54

8. Lee,S.M., Riley,E.M., Meyer,M.B., Benkusky,N.A., Plum,L.A., DeLuca,H.F. and Pike,J.W. (2015) 1,25-Dihydroxyvitamin D3 Controls a Cohort of Vitamin D Receptor Target Genes in the Proximal Intestine That Is Enriched for Calcium-regulating Components. *J. Biol. Chem.*, **290**, 18199–215.

9. Fletcher,M.N.C., Castro,M.A.A., Wang,X., de Santiago,I., O'Reilly,M., Chin,S.-F., Rueda,O.M., Caldas,C., Ponder,B.A.J., Markowetz,F., *et al.* (2013) Master regulators of FGFR2 signalling and breast cancer risk. *Nat. Commun.*, **4**, 2464.

10. Li,W., Notani,D., Ma,Q., Tanasa,B., Nunez,E., Chen,A.Y., Merkurjev,D., Zhang,J., Ohgi,K., Song,X., *et al.* (2013) Functional roles of enhancer RNAs for oestrogen-dependent transcriptional activation. *Nature*, **498**, 516–20.

11. Joseph,R., Orlov,Y.L., Huss,M., Sun,W., Kong,S.L., Ukil,L., Pan,Y.F., Li,G., Lim,M., Thomsen,J.S., *et al.* (2010) Integrative model of genomic factors for determining binding site selection by estrogen receptor-α. *Mol. Syst. Biol.*, **6**, 456.

12. Hu,M., Yu,J., Taylor,J.M.G., Chinnaiyan,A.M. and Qin,Z.S. (2010) On the detection and refinement of transcription factor binding sites using ChIP-Seq data. *Nucleic Acids Res.*, **38**, 2154–67.

13. He,H.H., Meyer,C.A., Chen,M.W., Jordan,V.C., Brown,M. and Liu,X.S. (2012) Differential DNase I hypersensitivity reveals factor-dependent chromatin dynamics. *Genome Res.*, **22**, 1015–25.

14. Brunelle,M., Nordell Markovits,A., Rodrigue,S., Lupien,M., Jacques,P.-É. and Gévry,N. (2015) The histone variant H2A.Z is an important regulator of enhancer activity. *Nucleic Acids Res.*, **43**, 9742–56.

Supplemental references

15. Franco,H.L., Nagari,A. and Kraus,W.L. (2015) TNFα signaling exposes latent estrogen receptor binding sites to alter the breast cancer cell transcriptome. *Mol. Cell*, **58**, 21–34.

16. Swinstead,E.E., Miranda,T.B., Paakinaho,V., Baek,S., Goldstein,I., Hawkins,M., Karpova,T.S., Ball,D., Mazza,D., Lavis,L.D., *et al.* (2016) Steroid Receptors Reprogram FoxA1 Occupancy through Dynamic Chromatin Transitions. *Cell*, **165**, 593–605.

17. Guertin,M.J., Zhang,X., Coonrod,S.A. and Hager,G.L. (2014) Transient estrogen receptor binding and p300 redistribution support a squelching mechanism for estradiol-repressed genes. *Mol. Endocrinol.*, **28**, 1522–33.

18. Hurtado,A., Holmes,K.A., Ross-Innes,C.S., Schmidt,D. and Carroll,J.S. (2011) FOXA1 is a key determinant of estrogen receptor function and endocrine response. *Nat. Genet.*, **43**, 27–33.